ACS OMEGA

http://pubs.acs.org/journal/acsodf

Article

Functional Group Characteristics and Pyrolysis/Combustion Performance of Karamay OS Based on FT-IR and TG−DTG Analyses

Wenlong Mo,* Xian-Kang Shan, Xiaoqiang He, Wen-Jie Qiang, Xian-Yong Wei, Bo Wei, Xing Fan, and Yulong Wu

Cite This: *ACS Omega* 2021, 6, 27684−27696

Read Online

ACCESS | Metrics & More | Article Recommendations

ABSTRACT: Proximate analysis, ultimate analysis, Fourier-transform infrared spectroscopy (FT-IR), and thermogravimetry−differential thermal analysis characterization were carried out on oily sludge (OS) samples OS1−OS5, from Karamay, Xinjiang, China. The Coast−Redfern model (CRm) was used to simulate the pyrolysis and combustion kinetics of oily samples. The results showed that the peak area percentage of benzene ring trisubstitution of OS5, in the range of 700−900 cm^{-1}, is close to 75%, corresponding to its high volatile content. Based on the kinetic analysis by the CRm, it is found that the fitting degree of the five samples is better when the reaction order is selected as $n = 2$, with R^2 close to 1.00 and $2RT/E$ to 0. Among them, the S_N and D_W of OS5 are $17.8 \times 10^{-10}\%^2$ min^{-2} $°C^{-3}$ and $0.10899 \times 10^{-5}\%$ min^{-1} $°C^{-2}$, respectively, higher than those of other samples, indicating a good combustion performance.

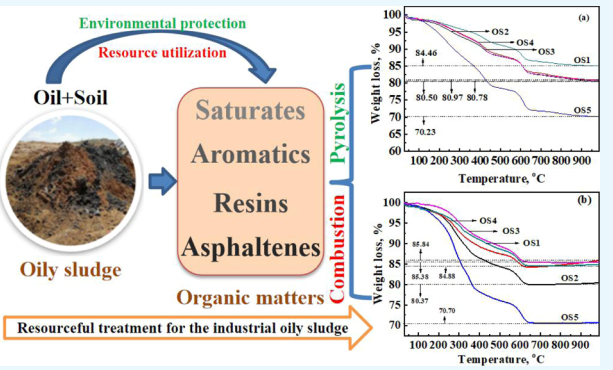

1. INTRODUCTION

Oily sludge (OS), known as oil-polluted soil, is the main solid pollutant in oil fields and related refining and chemical enterprises.[1] It has a complex and high heavy-oil composition. It contains benzene series, phenols, anthracene, toxic substances such as pyrene, and other harmful substances such as radionuclides.[2,3] Moreover, a large production of the OS will occupy a large amount of arable land, causing environmental pollution, such as soil, air, and water pollution. Therefore, reduction and resource utilization of the sludge has become one of the main contents of pollution control.[4,5] It is an important work for China and other countries to carry out ecological environment protection and develop circular economy.[6] Various methods including solvent extraction,[7] pyrolysis,[8] gasification,[9] and combustion[10] have been proposed. However, in the list of hazardous wastes issued and implemented, the solids treated by solvent extraction and incineration are still regulated as hazardous wastes, which limit the reduction of the sludge by the above two methods. As thermochemical processes, gasification, pyrolysis, and combustion are considered to be effective methods to treat OS.[11] By completely eliminating the pathogens, parasites, and other organic pollutants, the volume of the sludge can be effectively compressed. In addition, the sludge obtains energy in the form of heat, fuel oil, and syngas. Gasification has strict requirements on equipment, and the remaining garbage after gas production still needs subsequent treatment. Therefore, considering the scale and operability, pyrolysis/combustion have become promising technologies for OS resource utilization.

The pyrolysis technology refers to the process of transforming heavy organic components into light components through heating in the absence of oxygen.[12] Many factors affect the pyrolysis process. Gong et al.[13] found that as the temperature reached 200−580 °C, a large amount of volatile substances and light oil could be recovered from OS. Thus, the heating temperature has a great influence on the distribution and yield of the pyrolysis product. Presently, research studies on OS pyrolysis mainly focus on the relationship between the pyrolysis procedure and the corresponding product,[14−16] while the discussion on the pyrolysis mechanism and kinetics of OS is relatively less. It is also found that at lower heating rates (10, 20 K/min), the rate had little effect on the gas-phase yield, while at a higher rate (100 K/min), some volatile compounds would be released from OS immediately, greatly increasing the gas-phase yield.[17]

The pyrolysis of OS thermally converts heavy oil using high temperatures, so that the oil in OS is deeply cracked and

Received: May 25, 2021
Accepted: July 16, 2021
Published: October 11, 2021

Table 1. Proximate and Ultimate Analyses of OSs

	proximate analysis w/%				ultimate analysis w_{daf}/%				
sample	M_d	A_d	V_d	FC_d	C	H	N	S	H/C
OS1	3.01	80.07	14.12	2.80	77.69	16.95	1.59	3.77	2.63
OS2	3.44	78.10	17.48	0.98	81.80	13.83	1.39	2.99	2.03
OS3	3.07	75.66	17.54	3.73	80.02	15.72	1.41	2.84	2.36
OS4	3.09	77.12	19.82	0.00	80.21	14.70	1.38	3.71	2.20
OS5	3.50	71.35	25.64	0.00	84.01	12.38	1.13	2.47	1.77

recovered. It not only meets the requirements for high-value utilization of resources[18] but also achieves harmless "zero emissions". Under the premise of environmental protection, the OS pyrolysis technology provides a strong technical support for promoting sustainable economic development.[19] At the same time, the combustion characteristics of OS are an important indicator for evaluating fuels. Through calculation, the sludge in a specific area can be pyrolyzed in a targeted manner in order to achieve the goal of high-value utilization of OS.

In this paper, five OSs with different volatile contents from Karamay in Xinjiang, China, were taken as raw materials. By Fourier-transform infrared (FT-IR) spectroscopy characterization and thermogravimetry (TG) test, functional group characteristics of the samples were investigated, and pyrolysis dynamics simulation analysis was carried out based on the Coast−Redfern model (CRm). Thus, the corresponding fitting equations were obtained under different pyrolysis/combustion temperature regions, and the dynamics simulation parameters were calculated to determine the appropriate reaction order.

2. EXPERIMENTAL SECTION

2.1. Raw Materials. Five OSs (air-dry base) with different volatile contents from Karamay, Xinjiang, China (labeled OS1, OS2, OS3, OS4, and OS5) were used as raw materials in this experiment. Before the experiment, the sludges were screened and taken with the size of less than 80 mesh for standby.

2.2. Analysis Methods. Proximate analysis, ultimate analysis, FT-IR spectroscopy, and TG−DTG (derivative TG) characterization were carried out on five OSs. GB/T212-91 was used for proximate analysis, a Vario EL III element analyzer was used for ultimate analysis, FT-IR spectra were recorded with a TENSOR 27 infrared spectrometer, and TG/DTG was performed using an SDT Q600 TG analyzer. The pyrolysis behavior of OS1−OS5 was detected by heating the system from room temperature to 1253 K at a rate of 5 K/min with nitrogen as the carrier gas. The combustion behavior of the samples was tested with air as the carrier gas under the same conditions.

2.3. Kinetic Study. CRm[20−22] was used to simulate the pyrolysis and combustion kinetics of the oily samples. For the calculation method of this model, readers can refer to the previous work of Mo et al.[20]

2.4. Combustion Characteristic Analysis. As a comprehensive factor reflecting the characteristics of fuel ignition and burnout, it is generally believed that the bigger the value of the comprehensive combustion characteristic index (S_N), the better the combustion performance of the fuel. The combustion stability index (D_W) is used to evaluate the stability of the fuel. With the increase of D_W, the burning fuel is more stable;[23−25] for the calculation methods of the two indexes, refer to the previous work of our team.[20]

3. RESULTS AND DISCUSSION

3.1. Proximate and Ultimate Analyses. Table 1 shows the proximate and ultimate analyses data for the five OSs. From the table, it can be observed that the moisture (M_d) content of the five samples ranged from 3.0 to 3.5%, showing less water abundance. Volatile matter (V_d) in the five sludges differs from 14.12 to 25.64%, with OS1 showing a lower volatile abundance and OS5 presenting a higher abundance, and organic matter in volatile matter can be released during the pyrolysis process. The ash content (A_d) of each sample is high with values of above 70%, which is derived from the fact that the selected sludge sample is ascribed to the floor sludge, showing a much higher ash content than that of the tank bottom OS.[1]

Ultimate analysis shows that the content of C in OS1 is lower with a value of 77.69%, and OS5 shows a higher C abundance, and the C content in others is about 80%. The content of the H element is between 12 and 17%, indicating that the organic matter in OS is mainly composed of light organic matter, with a high H/C ratio of 1.75−2.75, and the organics might be chain-structured compounds, such as saturated chain alkanes. In addition, the H/C ratio of OS5 is smaller than that of the others, which may be due to its cyclic structures, including cycloalkanes or aromatics. Besides, the organic matter in OS contains higher N and S elements, and the content of S is as high as 2.40−3.80%. Volatile organic matter and N and S elements exhibit a serious impact on our environment, and the OS must be treated to remove the organic matter before reutilization in the soil.

From the relative content of V_d given in Table 1, it can be seen that OS5 > OS4 > OS3 > OS2 > OS1. Because the pyrolysis reaction mainly involves the thermal decomposition of organic matter in sludge, the final pyrolysis weight loss (WL) of the five samples is estimated to be on the order of OS5 > OS4 > OS3 > OS2 > OS1.

3.2. FT-IR Analysis. *3.2.1. FT-IR Spectrum.* Figure 1 presents the FT-IR spectra of OS1−OS5 samples. The

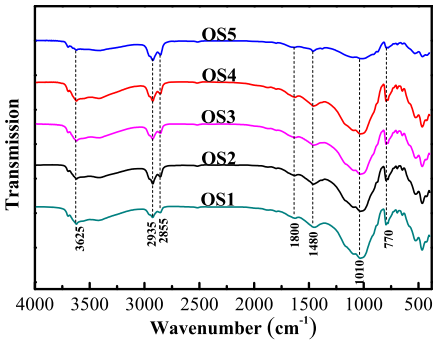

Figure 1. FT-IR profiles of the OS1-OS5 samples.

https://doi.org/10.1021/acsomega.1c02734
ACS Omega 2021, 6, 27684−27696

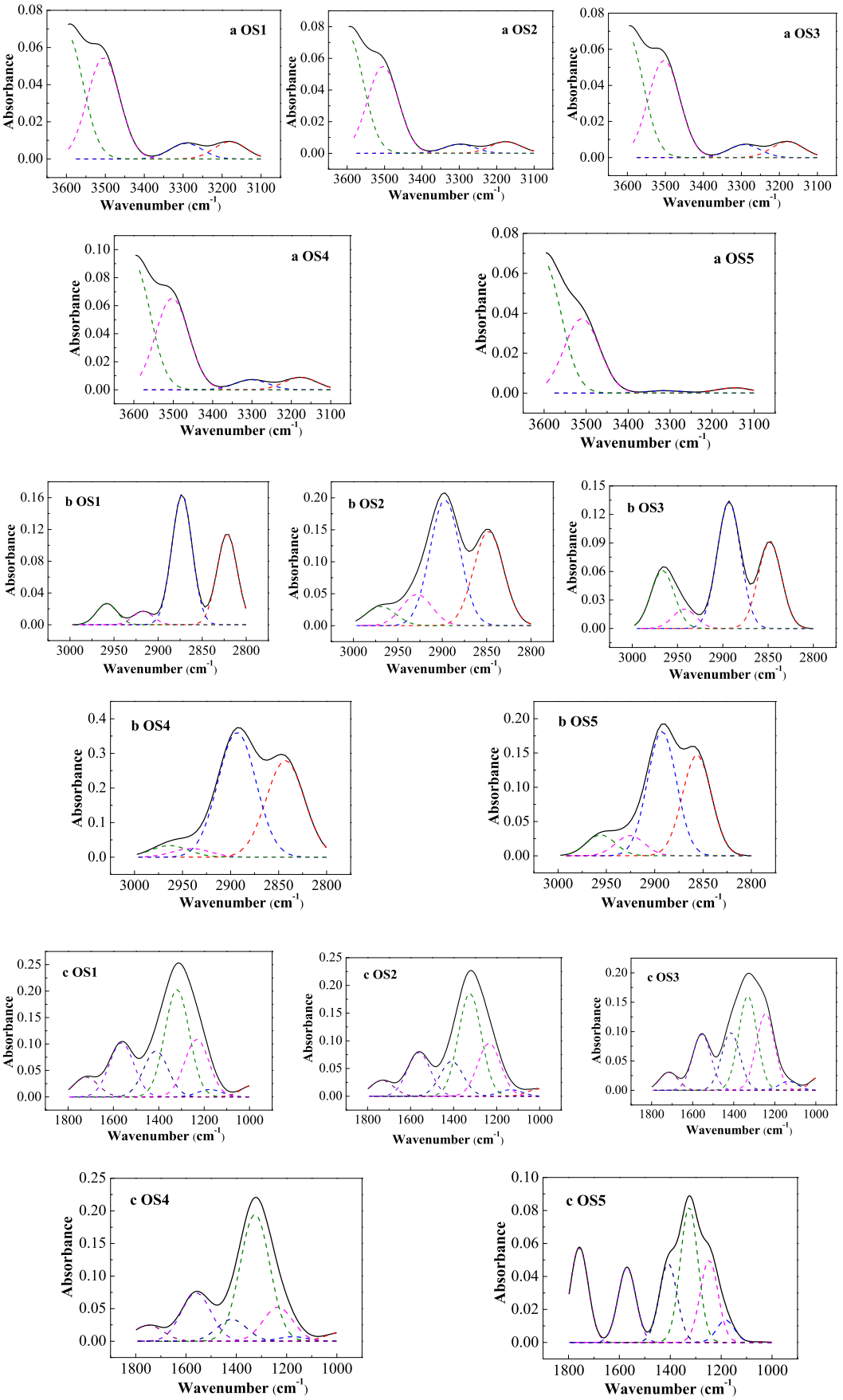

Figure 2. continued

https://doi.org/10.1021/acsomega.1c02734
ACS Omega 2021, 6, 27684−27696

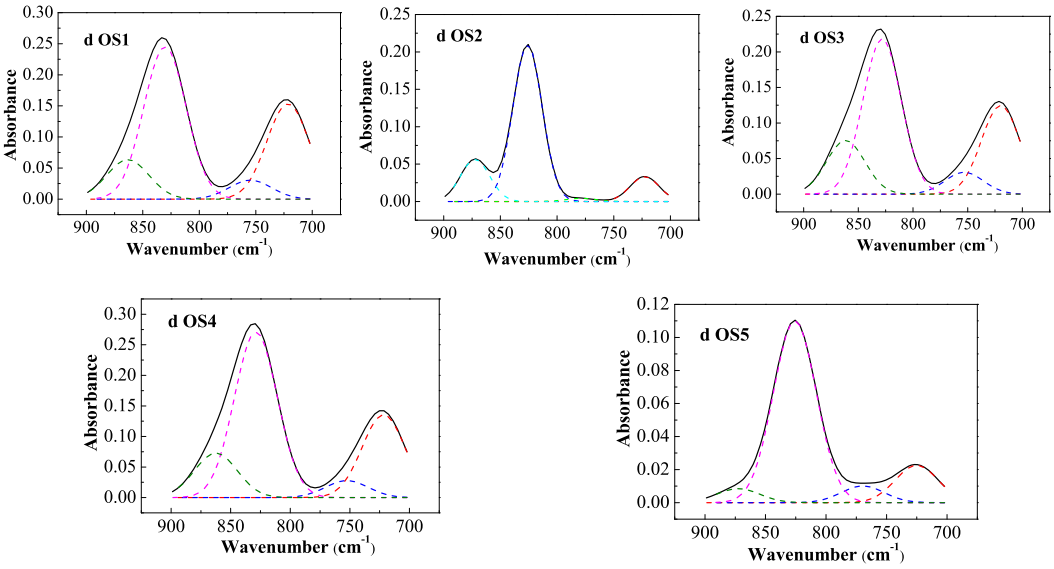

Figure 2. FT-IR curve-fitting results of the OS samples.

Table 2. Distribution of Functional Groups in Five OS Samples

band position/cm^{-1}	functional group	area percentage/%				
		OS1	OS2	OS3	OS4	OS5
3600−3500	OH-π	8.58	6.70	8.34	6.86	3.22
3500−3350	self-associated OH	8.04	5.47	7.04	5.81	1.71
3350−3260	OH-ether O	51.30	51.85	52.01	52.16	51.52
3260−3170	cyclic OH	32.08	35.98	32.61	35.17	43.55
2950	aliphatic $-CH_3$	34.85	34.98	29.89	39.67	37.83
2920	asymmetric aliphatic $-CH_2$	51.41	46.66	43.62	52.16	46.73
2890	aliphatic −CH	5.31	11.60	6.69	3.58	7.61
2850	symmetric aliphatic $-CH_2$	8.43	6.76	19.80	4.59	7.83
1690	carboxylic acids C═O	1.40	1.40	1.30	1.32	0.12
1560	aromatic C═C	2.49	2.49	2.85	1.79	4.68
1440	asymmetric CH_3-, CH_2-	19.52	20.47	24.27	13.54	17.21
1350	CH_3-Ar, R	36.38	39.65	29.88	50.34	28.28
1245	symmetric deformation $-CH_3$	15.62	13.56	18.33	8.71	16.49
1165	C−O phenols	18.41	16.97	17.84	19.28	15.74
1090	grease C−O	6.18	5.46	5.53	5.02	17.48
900−860	one adjacent H deformation	27.95	10.49	24.61	24.06	13.74
860−810	two adjacent H deformations	6.49	1.42	7.15	5.68	6.79
810−750	three adjacent H deformations	52.38	69.65	50.91	55.62	74.16
750−720	four adjacent H deformations	13.18	18.44	17.33	14.64	5.31

absorption peak between 3200 and 3600 cm^{-1} is ascribed to the hydroxyl group,[26] and the peak at 3625 cm^{-1} is attributed to the OH−π bond. The hydroxyl group is easily hydrogen bonded, which may lead to a "blue shift", that is, the self-associated −OH stretching vibration absorption peak around 3300 cm^{-1} shifted in the vicinity of 3625 cm^{-1}. The peak at 2850−2950 cm^{-1} is attributed to the stretching vibration of the C−H bond, such as aliphatic structures, $-CH_3$, $-CH_2$, and −CH,[27−29] indicating that there are more aliphatic organic compounds in the sample. The peak around 1800 cm^{-1} is assigned to the C═O bond, indicating that each sample may contain ketones, aldehydes, acids, and other C═O bond-containing substances, and the weak absorption peak represents that the relative abundance of the above three types of organic matter is relatively less. The peak at 1480 cm^{-1} is ascribed to the vibration absorption of the aromatic structure, which is weaker for OS5, demonstrating that the aromatic species/content of OS5 is less than other samples. At 1010 cm^{-1}, the absorption peak of the C−O bond was found, and the abundance of OS5 was the weakest. At 770 cm^{-1}, there is an out-of-plane bending vibration absorption peak attributed to the benzene ring for each OS, and the strength of the OS5 sample is weaker, which is consistent with the weak vibration absorption peak of the aromatic ring skeleton observed at 1480 cm^{-1}.

3.2.2. FT-IR Semi-Quantitative Analysis. According to the types of functional groups, the infrared spectrum can be divided into four regions, 3100−3600, 2800−3000, 1000−1800, and 700−900 cm^{-1}.[30−32] PeakFit software was used to fit the infrared spectrum for the four regions, and semi-quantitative analysis was conducted to understand the type and distribution of the functional group of the organic matter in OS.[33−36] The peak fitting results are shown in Figure 2a−d and Table 2. The absorption peak of the hydroxyl functional group

https://doi.org/10.1021/acsomega.1c02734
ACS Omega 2021, 6, 27684−27696

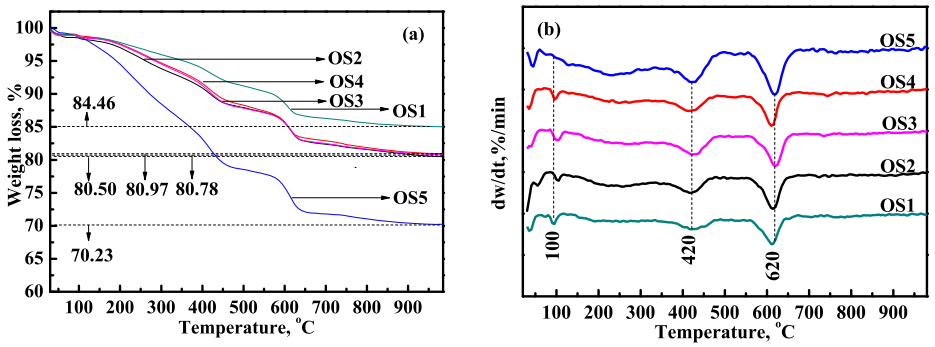

Figure 3. TG−DTG profiles of the OS1-OS5 samples: (a) TG and (b) DTG curves.

of each OS is mainly distributed in the 3100−3600 cm^{-1} region (Figure 2a), which exists mainly in four forms: the hydroxyl π bond, self-associating hydroxyl hydrogen bond, hydroxyl ether hydrogen bond, and hydroxyl cyclic hydrogen bond. The positions of infrared absorption peaks for the five samples within this wavelength range are basically the same, indicating that the hydroxyl functional groups in the five samples are basically the same. From the peak area percentage, the hydroxyl groups in residues are mainly the hydroxyl ether hydrogen bond and the hydroxyl cyclic hydrogen bond, with a total relative abundance of more than 80%. In addition, the proportion of the hydroxyl ether hydrogen bond is high with a value of 52%, while the self-associating hydroxyl hydrogen bond is just low with a value of 8%.

From Figure 2b, aliphatic CH_X absorption peaks appearing in the range of 2800−3000 cm^{-1} can be divided into four subpeaks. As can be seen from Table 2, the $-CH_X$ absorption peak is dominated by aliphatic $-CH_3$ and asymmetric aliphatic $-CH_2$, with the sum area percentage of 70−90%, and the content of asymmetric $-CH_2$ is higher than 45%. It is also known that the peak area of C═O from carboxylic acid at 1690 cm^{-1} varies little, demonstrating that the carboxylic acid structure in the sample is relatively stable. The OS5 sample shows a higher grease C−O content at 1090 cm^{-1} and higher $-CH_3$ abundance on the aromatic ring at 1350 cm^{-1}. According to the peak area percentage data in the fingerprint area in the table, benzene ring triple substitution is the main structure in the range of 700−900 cm^{-1}, accounting for more than 50%, and OS5 also shows a higher relative abundance, accounting for nearly 75%, resulting from its high V_d.

3.3. Pyrolysis Performance of OS. *3.3.1. Pyrolysis Characteristics.* Figure 3 presents the TG−DTG profiles of OS1-OS5 samples. From the TG diagram, the WL of OS1 is observed to be lower with a value of 16%, while the loss of the OS5 sludge is up to 30%, and the loss of the other three sludge samples is not much different and around 20%. According to proximate analysis, the V_d of OS1 is 14.12%, which is about 18% for OS2−OS4 and OS5 shows a higher V_d of 25.64%. Therefore, the higher the volatile matter in the sludge sample, the greater the WL, and the WL for each sample is slightly higher than the volatile value, which is related to the experimental conditions for TG characterization and volatile test. TG characterization requires 50−100 mg of sample under an atmosphere of nitrogen flow, while the volatile test needs 1.00 g of sample without gas flow. A small amount of sample is more conducive to heat transfer, resulting in a higher proportion of substances escaping from the sludge at the same temperature. According to the data calculation in Figure 3a, the final WL values of OS1−OS5 are 15.54, 19.03, 19.22, 19.50, and 29.77%, respectively. The size order is OS5 > OS4 > OS3 > OS2 > OS1. These results are consistent with the inferred results presented in Section 3.1.

As shown in Figure 3b, the pyrolysis process of the OS1−OS5 samples could be divided into four stages: removal of N_2, O_2, CH_4, and other small-molecular gases (<75 °C), evaporation of water (75−150 °C), release of volatile matter (150−475 °C), and the decomposition reaction of complex organic matter (475−650 °C), respectively. The separation process of sludge and oil in OS mainly occurs at 200−650 °C.[37,38] Some oil samples evaporate at high temperatures because of their high boiling points.

From the TG curves of OS1−OS5 in Figure 3a,b, it can be concluded that oil separation in the studied OSs mainly occurred between 150 and 650 °C. Among the four stages, the first two stages correspond to the escape of small-molecule gases and moisture from OS. The third stage is the low-temperature stage, when organic matter decomposition occurs and a large amount of volatile substances are released, containing fats, proteins, and sugars in the OS, and for these three components, the priority of decomposition is fat (200−300 °C), protein (300−390 °C), and sugars above 390 °C.[39] The fourth stage was the high-temperature stage of the sludge pyrolysis. At this stage, the mass loss of OS1−OS5 was 5.05, 5.51, 5.11, 5.27, and 6.91, which were all higher than the fixed carbon (FC_d) content in OSs, as shown in Table 1. This is due to the decomposition reaction that may be accompanied by the reaction of complex organic components. After 650 °C, the pyrolysis process of the organic matter is basically completed, followed by the decomposition of minerals in the sludge, with little change in the WL rate.

3.3.2. Thermal Analysis (DTA). From the DTA curves in Figure 4, it can be seen that the DTA values of five samples were less than zero, demonstrating that the pyrolysis process of OS mainly occurred as an endothermic reaction. The temperature of the maximum DTA value is around 650 °C for all the five samples, indicating that the reaction heat effect is most obvious at this time. In addition, it may be concluded that more heat needs to be provided to crack the cyclic organic compounds in OS. Furthermore, the DTA value of the OS5 sample is larger by about −27 mV/mg, which might be related to its larger volatile abundance, containing more complex organics.

3.3.3. Conversion−Temperature Relationship. Figure 5 shows the relationship between pyrolysis conversion and temperature. As shown in the figure, the pyrolysis process can be divided into four stages according to the conversion−

https://doi.org/10.1021/acsomega.1c02734
ACS Omega 2021, 6, 27684−27696

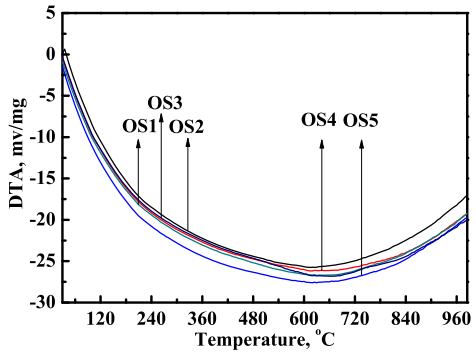

Figure 4. DTA profiles of the OS1-OS5 samples.

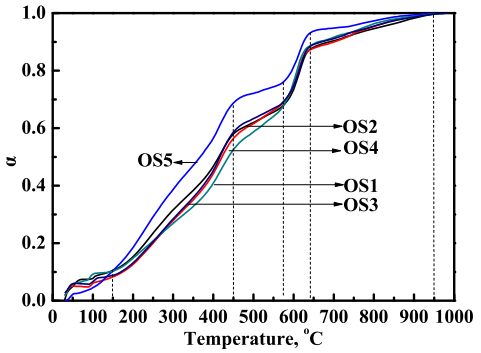

Figure 5. Conversion−temperature profiles of the five OS samples.

temperature relationship, with the temperature regions of 150−450, 450−575, 575−640, and 640−950 °C, respectively. From the DTG profile, it can be seen that the temperature of the maximum weightlessness rate peak for all the sludge samples is located in the third stage, indicating that the pyrolysis process in this section is more serious, followed by the first stage, with the slope near the third one.

According to CRm, parameters corresponding to the pyrolysis process in four temperature stages with the reaction order n equal to 1−3 were calculated, and the fitting graphs are presented as Figures 6−8.

The kinetic parameters of each sludge sample calculated by CRm are shown in Table 3.

Table 3 shows that with the increase of the reaction order, the activation energy calculated from sludge samples OS1−OS5 shows an upward trend, indicating that the higher the reaction order is, the more complex the simulated pyrolysis process. It is more advantageous to release small molecules from the sludge sample in the lower-temperature stage (<575 °C), as lower activation energy is required, while the organic matter that is difficult to dissociate in the higher-temperature stage requires higher activation energy to escape and/or undergo decomposition. In addition, the coking of organic matter during the pyrolysis of OS may produce a higher activation energy of about 900 °C, and due to the large difference in the content and type of organic components, the activation energy of coking is also very different.

In the first temperature interval, as the reaction order increases, the correlation coefficient R^2 shows a downward trend. According to the assumption of $2RT/E \rightarrow 0$, obtained by the Coast−Redfern simulation method, when the reaction order $n = 1$, the simulation effect of the pyrolysis process of the OS1−OS5 samples is poor. Therefore, the reaction order of the first temperature interval $n = 2$ is more appropriate, the pyrolysis activation energy is almost all below 17 kJ/mol. In the second temperature interval, the comparison correlation coefficient $R^2 \rightarrow 1$ and $2RT/E \rightarrow 0$. The fitting effect of the five samples is poor. In the third temperature interval, comparing the data in the table, when the reaction order $n = 2$, the fitting effect is the best, which tends to the hypothetical conditions, and activation energy is in the range of 110−140 kJ/mol. When $n = 3$, the second assumption of the OS5 sample has a large deviation. In the fourth temperature range, the fitting effect is best when $n = 3$ and the activation energy is between 115 and 195 kJ/mol. When $n = 2$, the fitting effect is slightly weaker. Based on the above analysis, when $n = 2$ is used for pyrolysis kinetic fitting, the fitting results are more suitable than other reaction orders in the four temperature ranges.

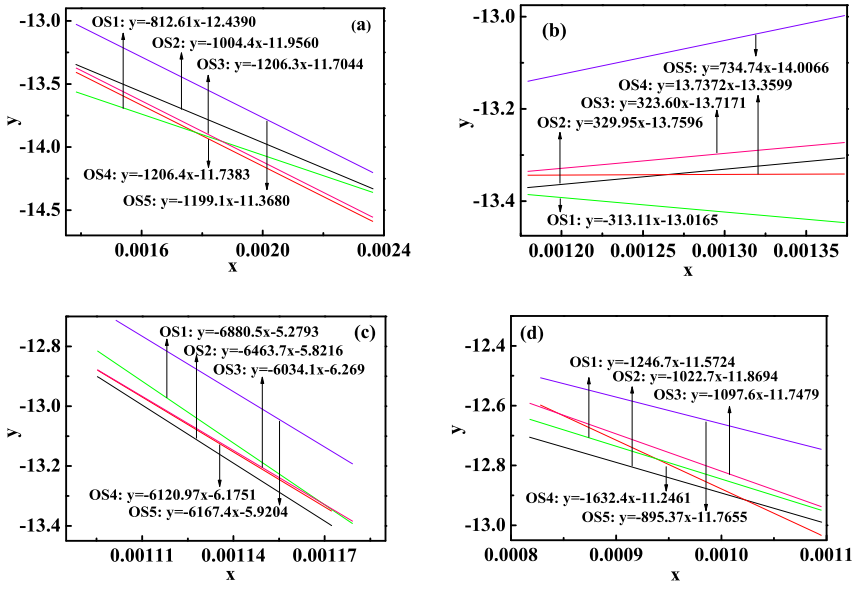

Figure 6. Pyrolysis kinetic fitting profiles of OS samples for $n = 1$. (a) 423−723; (b) 723−848; (c) 848−913; and (d) 913−1223 K.

https://doi.org/10.1021/acsomega.1c02734
ACS Omega 2021, 6, 27684−27696

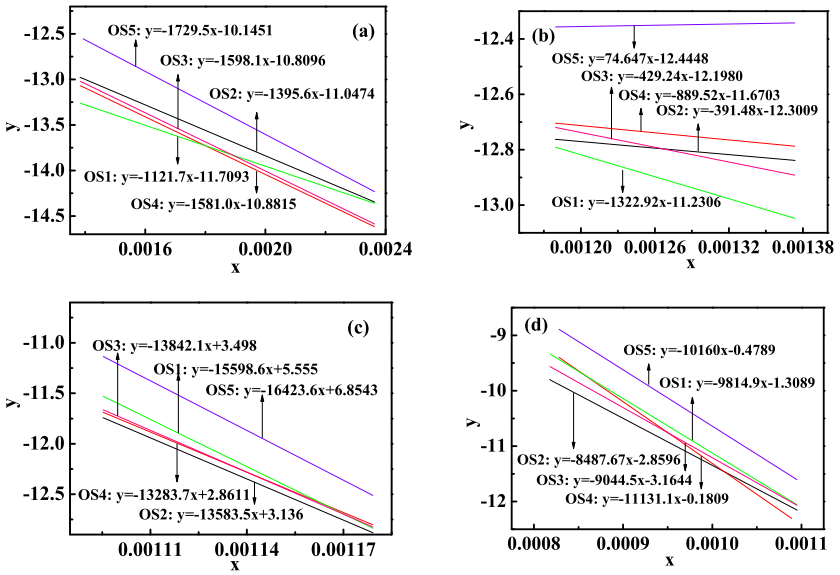

Figure 7. Pyrolysis kinetic fitting profiles of OS samples for n = 2. (a) 423−723; (b) 723−848; (c) 848−913; and (d) 913−1223 K.

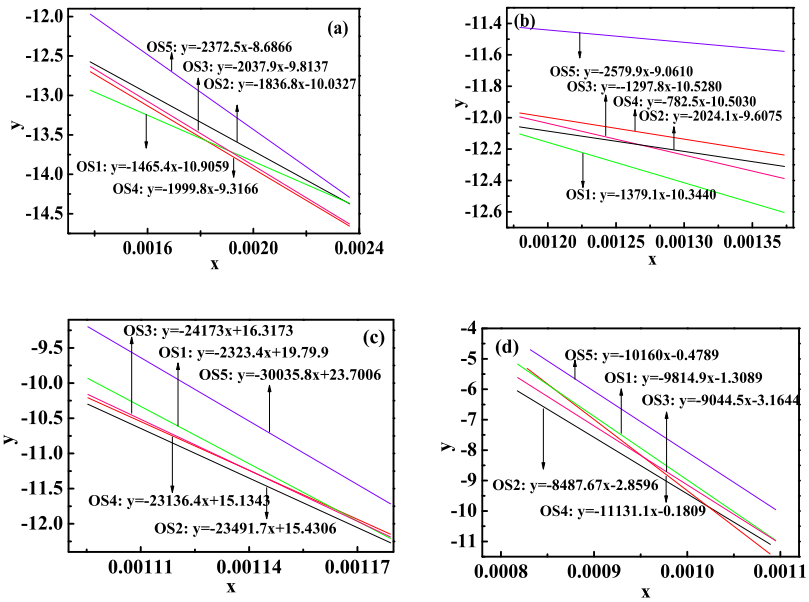

Figure 8. Pyrolysis kinetic fitting profiles of OS samples for n = 3. (a) 423−723; (b) 723−848; (c) 848−913; and (d) 913−1223 K.

3.4. Combustion Characteristic Analysis. *3.4.1. Combustion Characteristics.* Figure 9 presents the combustion TG−DTG profiles of OS1−OS5 samples with air as the test atmosphere. From the TG diagram, the WL of OS5 is determined to be around 30%, which lowered to 20% for OS2, and the loss of other sludge samples is not much different and less than 16%. Combustible components in the sludge include V_d and FC_d, the sum of which in OS1−OS5 is 16.92, 18.46, 21.27, 19.82, and 25.64%, respectively. Obviously, the combustion WL values of OS2 and OS5 are higher than the corresponding sum of V_d and FC_d, while OS1, OS3, and OS4 are the opposite. The above results indicate that there is no strict correlation between the combustion WL and the sum of V_d and FC_d, which might be derived from the existence of other combustible materials or from the catalytic effect of inorganic matter in the sample.[40]

It can be seen from the DTG profile that there are three obvious WL rate peaks that appeared in the combustion process of each sludge sample. The first peak, located around 105 °C, is caused by the heat removal of the adsorbed small molecules, such as N_2, O_2, CH_4, H_2O, and so forth, and the peak may also be attributed to the dehydration and drying of the sludge sample. The second one, at about 315 °C, is assigned to the severe decomposition and escape of the organic matter, during which a large amount of V_d is released and the combustion reaction might have taken place. On the other hand, DTG diagrams fluctuate obviously, and there are two loss rate peaks appearing in the profiles for the samples of OS2 and OS5 around 315 °C, which may be attributed to the large WL of the two samples. In addition, V_d emission from the solid might conform to the "shrinking-core model". The volatile molecules on the surface of the sludge particle are first heated (around 250 °C) to escape and burn and then, the heat generated is transferred into the inner layer or pore of the particles, while the inner volatiles need to cross the surface layer and overcome the diffusion resistance to contact with

https://doi.org/10.1021/acsomega.1c02734
ACS Omega 2021, 6, 27684−27696

Table 3. Pyrolysis Kinetic Parameters of OS Samples

T/K	samples	reaction order	regression equation	correlation coefficient R^2	activation energy E/(kJ/mol)	pre-exponential factor A/min^{-1}	$2RT/E$
423−723	OS1	1	$y = -812.61x - 12.4390$	0.9756	6.76	1.61×10^{-2}	1.1075
		2	$y = -1121.7x - 11.7093$	0.9604	14.38	3.40×10^{-1}	0.5204
		3	$y = -1465.4x - 10.9059$	0.9432	12.18	1.34×10^{-1}	0.6142
	OS2	1	$y = -1004.4x - 11.9560$	0.9858	8.35	3.22×10^{-2}	0.8961
		2	$y = -1395.6x - 11.0474$	0.9834	79.30	4.29×10^{6}	0.0734
		3	$y = -1836.8x - 10.0327$	0.9706	15.27	4.04×10^{-1}	0.4900
	OS3	1	$y = -1206.3x - 11.7044$	0.9895	10.03	4.98×10^{-2}	0.7461
		2	$y = -1598.1x - 10.8096$	0.9762	9.33	4.61×10^{-2}	0.8024
		3	$y = -2037.86x - 9.8137$	0.9575	16.94	5.57×10^{-1}	0.4416
	OS4	1	$y = -1206.4x - 11.7383$	0.9912	10.03	4.81×10^{-2}	0.7460
		2	$y = -1581.0x - 10.8815$	0.9829	11.60	1.11×10^{-1}	0.6449
		3	$y = -1999.8x - 9.3166$	0.9676	16.63	8.99×10^{-1}	0.4500
	OS5	1	$y = -1199.1x - 11.3680$	0.9789	9.97	6.93×10^{-2}	0.7506
		2	$y = -1729.5x - 10.1451$	0.9884	13.14	1.49×10^{-1}	0.5693
		3	$y = -2372.5x - 8.6866$	0.9747	19.72	2.00×10	0.3793
723−848	OS1	1	$y = -313.11x - 13.0165$	0.8567	2.60	3.48×10^{-3}	3.6728
		2	$y = -1322.9x - 11.2306$	0.9619	0.62	1.47×10^{-3}	0.4100
		3	$y = -1379.1x - 10.3440$	0.9683	11.47	2.22×10^{-1}	0.8339
	OS2	1	$y = 329.95x - 13.7596$	0.9618	2.74	1.74×10^{-3}	3.4854
		2	$y = -391.48x - 12.3009$	0.8802	13.29	1.61×10^{-1}	0.5632
		3	$y = -2024.1x - 9.6075$	0.9773	16.83	6.80×10^{-1}	0.5682
	OS3	1	$y = 323.60x - 13.7171$	0.9438	2.69	-1.79×10^{-3}	−3.5530
		2	$y = -429.24x - 12.1980$	0.8917	11.00	8.77×10^{-2}	0.8693
		3	$y = -1297.8x - 10.5280$	0.9645	10.79	1.74×10^{-1}	0.8861
	OS4	1	$y = 13.7368x - 13.3599$	0.0110	0.11	-1.08×10^{-4}	−83.7100
		2	$y = -889.52x - 11.6703$	0.9623	3.25	8.90×10^{-3}	2.9376
		3	$y = -782.5x - 10.5030$	0.8913	6.51	1.07×10^{-1}	1.4696
	OS5	1	$y = 734.74x - 14.0066$	0.9869	6.11	-3.03×10^{-3}	−1.5650
		2	$y = 74.6467x - 12.4448$	0.1438	7.40	3.80×10^{-2}	1.2928
		3	$y = -2579.9x - 9.0610$	0.9711	21.45	1.50×10	0.4458
848−913	OS1	1	$y = -6880.5x - 5.2793$	0.9754	57.20	1.75×10^{2}	0.1860
		2	$y = -15598.6x + 5.5550$	0.9779	136.55	7.78×10^{7}	0.0779
		3	$y = -2323.4x + 19.7909$	0.9768	19.23	4.55×10^{12}	0.5533
	OS2	1	$y = -6463.7x - 5.8216$	0.9688	53.74	9.58×10^{1}	0.1980
		2	$y = -13583.5x + 3.1360$	0.9520	112.93	1.57×10^{6}	0.1249
		3	$y = -23491.7x + 15.431$	0.9489	195.31	5.91×10^{11}	0.0545
	OS3	1	$y = -6034.1x - 6.2690$	0.9536	50.17	5.71×10^{1}	0.2121
		2	$y = -13842.1x + 3.4980$	0.9480	129.69	2.02×10^{7}	0.0821
		3	$y = -24173x + 16.3173$	0.9445	200.97	1.48×10^{12}	0.0530
	OS4	1	$y = -6120.97x - 6.1751$	0.9679	50.89	6.37×10^{1}	0.2091
		2	$y = -13283.7x + 2.8612$	0.9645	112.93	1.56×10^{6}	0.0942
		3	$y = -23136.4x + 15.134$	0.9637	192.36	4.32×10^{11}	0.0553
	OS5	1	$y = -6167.4x - 5.9204$	0.9454	51.28	8.28×10^{1}	0.2075
		2	$y = -16423.6x + 6.8543$	0.9480	110.44	1.16×10^{6}	0.0964
		3	$y = -30035.8x + 23.701$	0.9445	249.72	2.95×10^{15}	0.0426
913−1223	OS1	1	$y = -1246.7x - 11.5724$	0.8386	81.60	4.62×10^{-1}	0.1936
		2	$y = -9814.9x - 1.3089$	0.8880	84.47	3.15×10^{4}	0.1870
		3	$y = -9814.90x - 1.3089$	0.8962	173.81	1.58×10	0.0909
	OS2	1	$y = -1022.7x - 11.8694$	0.5704	70.57	2.97×10^{-1}	0.2239
		2	$y = -8487.6x - 2.8596$	0.7703	115.08	2.29×10^{6}	0.0925
		3	$y = -8487.67x - 2.8596$	0.7934	154.40	8.60×10^{8}	0.1023
	OS3	1	$y = -1097.6x - 11.7479$	0.7351	75.20	3.58×10^{-1}	0.2101
		2	$y = -9044.5x - 2.1644$	0.8477	81.60	1.33×10^{4}	0.1936
		3	$y = -9044.5x - 3.1644$	0.8611	160.98	2.66×10^{9}	0.0981
	OS4	1	$y = -1632.4x - 11.2461$	0.7434	92.54	7.27×10^{-1}	0.1707
		2	$y = -11131.1x - 0.1809$	0.7961	70.57	2.43×10^{3}	0.2239
		3	$y = -11131.1x - 0.1809$	0.8083	194.17	1.44×10^{11}	0.0814
	OS5	1	$y = -895.37x - 11.7655$	0.4170	84.47	3.95×10^{-1}	0.1870
		2	$y = -10160.0x - 0.4789$	0.7068	92.54	4.64×10^{4}	0.1707
		3	$y = -10160x - 0.4789$	0.8258	165.83	1.45×10	0.0953

https://doi.org/10.1021/acsomega.1c02734
ACS Omega 2021, 6, 27684−27696

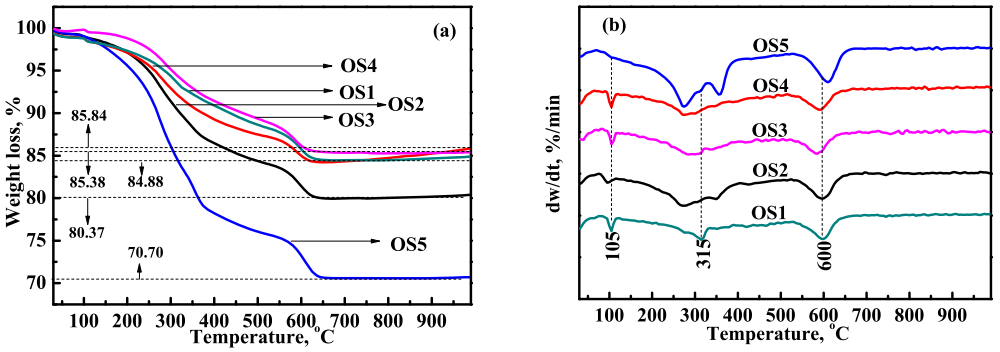

Figure 9. Combustion TG–DTG profiles of OS1–OS5 samples: (a) TG and (b) DTG.

oxygen or air for combustion, thus the required temperature would be higher. It is worth noting that the maximum WL rate peak temperature of all the sludge samples is around 600 °C, which might be attributed to the rapid combustion of non-volatile organic matter in the sludge, or the violent oxidation reaction of FC_d. After 650 °C, the combustion process is basically completed, with little change in the WL rate.

3.4.2. Combustion Characteristic Index. The ignition temperature and the burnout temperature of five OSs were determined by the tangent method,[41,42] the initial combustion temperature (T_i) reflects the combustion performance of the fuel, the smaller the T_i, the easier the fuel will catch fire. The burnout temperature (T_f) represents the final temperature that can be reached when the combustible materials in the fuel are burned out. Take Figure 10 as an example for analysis. At the

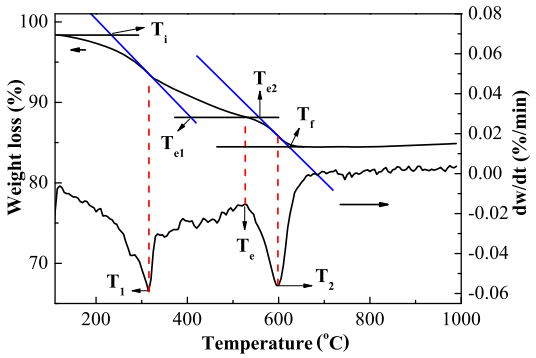

Figure 10. Parameter analysis of the OS1 combustion profile.

first peak point of WL rate, T_1, of the DTG curve, a vertical line is made to intersect the TG curve, and the tangent of the intersection point intersects the upper horizontal tangent of the TG curve. The temperature at this time is defined as T_i. Similarly, at the second peak point of WL rate, T_2, of the DTG curve, a vertical line is made to intersect the TG curve, and the tangent of the intersection point intersects the lower horizontal tangent of the TG curve to obtain T_f, as shown in Figure 10. In the TG curve, a horizontal line is made at the inflection point T_e, and T_{e1} and T_{e2} are obtained by crossing the first and second tangent lines. The combustion process is divided into three stages: the volatile combustion stage ($T_i - T_{e1}$), combustion transition stage ($T_{e1} - T_{e2}$), and coke combustion stage ($T_{e2} - T_f$).[43−45]

T_i and T_f of the other four sludges were also determined by the tangent method, and the values of S_N and D_W were calculated; the results are shown in Table 4. The bigger the S_N value was, the better the combustion quality was.[46] Based on

Table 4. Combustion Characteristic Index of Different Samples

samples	T_i (°C)	T_f (°C)	$(dw/dt)_{max}$ (% min^{-1})	$S_N \times 10^{-10}$ (%^{2} min^{-2} $°C^{-3}$)	$D_w \times 10^{-5}$ (% min^{-1} $°C^{-2}$)
OS1	232	625	0.05887	3.1	0.04060
OS2	201	626	0.07614	6.8	0.06118
OS3	218	614	0.05384	3.3	0.04022
OS4	203	617	0.05906	3.9	0.04715
OS5	202	633	0.13936	17.8	0.10899

this fact, compared with the other four sludge samples, the S_N value and D_W value of OS5 are higher with values of 17.8 × 10^{-10}%^{2} min^{-2} $°C^{-3}$ and 0.10899 × 10^{-5}% min^{-1} $°C^{-2}$, respectively, indicating that the sludge with a high volatile content presents a better comprehensive combustion performance (Figure 11).

3.4.3. Conversion–Temperature Relationship. Figure 12 shows the relationship between combustion conversion and temperature. Because the minerals in OS4 are oxidized in the oxygen atmosphere, the conversion rate α is greater than 1. This phenomenon also appears in the research results of Mo et al.[20] It can be seen from the figure that the slope of the combustion conversion at different temperature regions is quite different, demonstrating that the α-T profile in the figure can be divided into two stages with the temperature region of 150–375 and 375–650 °C, respectively. According to CRm, the combustion process is fitted by the reaction order of n = 1–3, as shown in Figures 13–15.

Correspondingly, the combustion kinetic parameters of each OS sample are calculated, as shown in Table 5. When the reaction order n = 1, the combustion activation energy for the five samples in the first stage is 13–25 kJ/mol, and the energy in the second stage is almost below 20 kJ/mol, lower than the value in the first stage for each sample. On the one hand, in the range of 150–375 °C, the difficult-to-dissociate organic matter in sludge samples will be cracked or condensed, resulting in the activation energy required for combustion being higher; while in the range of 375–650 °C, the activation energy required is lower, which may be due to the higher initial temperature required for fixed-carbon combustion; therefore, the combustion process does not require a higher activation energy. On the other hand, according to proximate analysis, there is almost no FC_d in OS4 and OS5, which is inconsistent with the combustion curve. The reason may be that FC_d in OS is tightly encapsulated by the soil and cannot be accurately identified by proximate analysis (with a test sample of 1.00 g). Although the amount of sample required for the thermogravimetric test is just 50–100 mg, the combustion process of FC_d can be

https://doi.org/10.1021/acsomega.1c02734
ACS Omega 2021, 6, 27684−27696

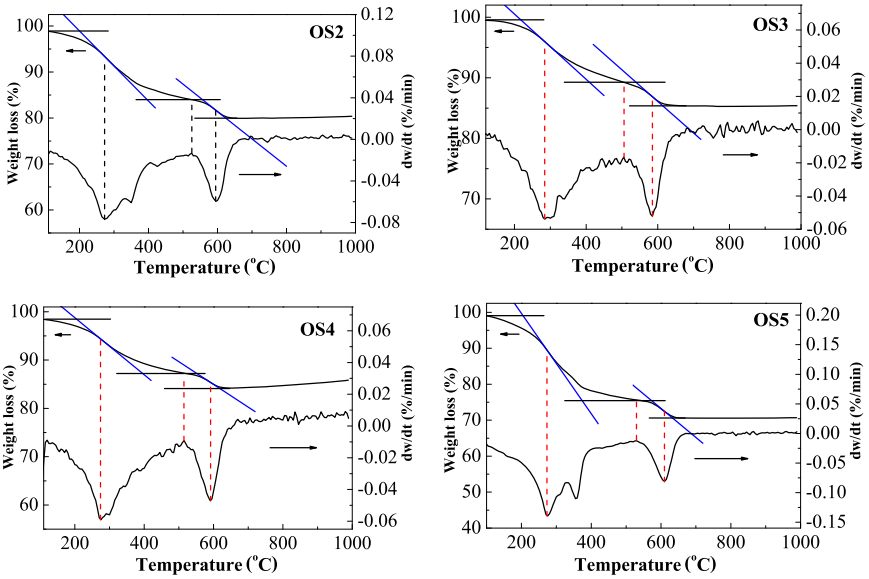

Figure 11. TG−DTG profiles of OS2-OS5 under an air atmosphere.

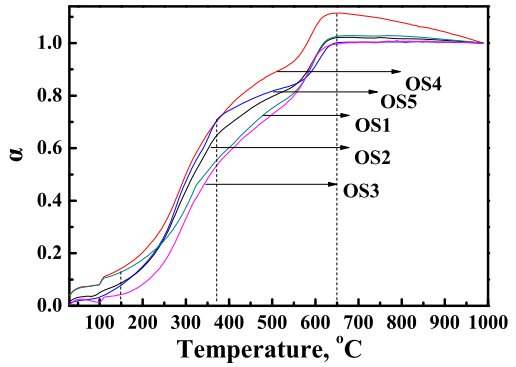

Figure 12. Conversion−temperature profiles of the five OS samples.

performed sufficiently in air flow. Data in the table also show that the value of R^2 of each sample in the second stage is higher than 0.5. According to the assumption that $2RT/E \rightarrow 0$ by the Coast−Redfern simulation model, it indicates that the simulation effect with reaction order $n = 1$ for the combustion process of the sludge sample, especially in the second stage, is poor.

Corresponding to the reaction order $n = 2$, the activation energy of each sample is almost higher than that of $n = 1$ for the two stages, and the increase of activation energy in the second stage is more obvious, with the value of energy, at $n = 2$, being more than 1 time higher than the first-order reaction model. A possible reason might be that the combustion reaction of organic matter with a complex condensation structure in OS or in pyrolysis char produced by the first heating stage needs a higher activation energy. On the other hand, the higher the reaction order, the more complex the simulated combustion process. From the data in the table, considering the assumption that $2RT/E \rightarrow 0$ and the value of $R^2 \rightarrow 1$, the fitting effect at $n = 2$ is better than that at $n = 1$.

With the reaction order of $n = 3$, the fitting effect under this reaction order is slightly better than that of $n = 2$, but the activation energy is obviously increased and the fitting reaction complexity is higher. Therefore, it can be considered that the combustion reaction order of the sludge samples is more appropriate at $n = 2$, with the activation energy of 15−30 kJ/mol at the low-temperature region and 40−60 kJ/mol at the high-temperature region. Based on the above analysis, when $n = 2$ is used for combustion kinetic fitting, the fitting results are more suitable than other reaction orders in the four temperature ranges.

4. CONCLUSIONS

The OS from Xinjiang Karamay (China) was characterized by proximate analysis, ultimate analysis, FT-IR, and TG−DTG tests. Proximate and ultimate analyses showed that the V_d of OS samples was about 15−25%, among which OS5 presented a higher V_d and C element abundance and a less H/C ratio. FT-IR spectra showed high $-CH_3$ and $-CH_2$ abundance at 1350 cm^{-1} due to the aromatic ring of the OS5 sample; a high

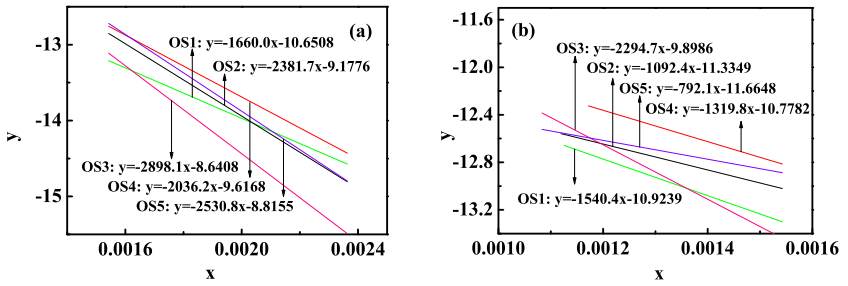

Figure 13. Combustion kinetic fitting profiles of OS samples for $n = 1$. (a) 423−648 and (b) 648−923 K.

https://doi.org/10.1021/acsomega.1c02734
ACS Omega 2021, 6, 27684−27696

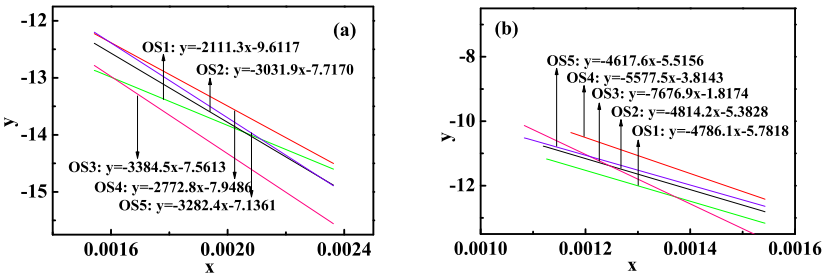

Figure 14. Combustion kinetic fitting profiles of OS samples for n = 2. (a) 423−648 and (b) 648−923 K.

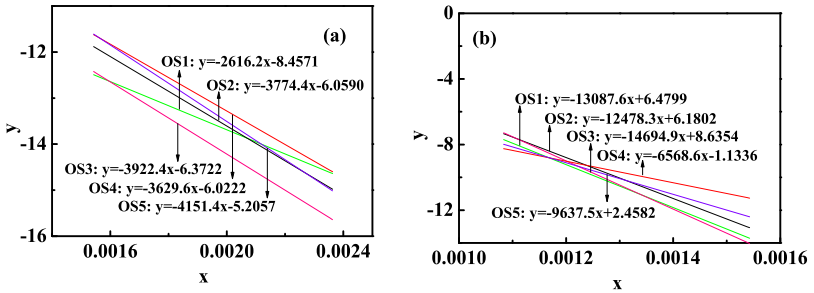

Figure 15. Combustion kinetic fitting profiles of OS samples for n = 3. (a) 423−648 and (b) 648−923 K.

Table 5. Combustion Kinetic Parameters of OS Samples

T/K	samples	reaction order	regression equation	correlation coefficient R^2	activation energy E/(kJ/mol)	pre-exponential factor A/min^{-1}	$2RT/E$
423−648	OS1	1	$y = -1660.0x - 10.6508$	0.9692	13.801	1.97×10^{-1}	0.5096
		2	$y = -2111.3x - 9.6117$	0.9550	17.554	7.07×10^{-1}	0.4007
		3	$y = -2616.2x - 8.4571$	0.9405	21.751	2.78×10	0.3234
	OS2	1	$y = -2381.7x - 9.1776$	0.9911	19.801	1.23×10	0.3552
		2	$y = -3031.9x - 7.7170$	0.9826	25.207	6.75×10	0.2790
		3	$y = -3774.4x - 6.0590$	0.9685	31.380	4.41×10^{1}	0.2241
	OS3	1	$y = -2898.1x - 8.6408$	0.9916	24.095	2.56×10	0.2919
		2	$y = -3384.5x - 7.5613$	0.9879	28.139	8.80×10	0.2500
		3	$y = -3922.4x - 6.3722$	0.9799	32.611	3.35×10^{1}	0.2157
	OS4	1	$y = -2036.2x - 9.6168$	0.9780	16.929	6.78×10^{-1}	0.4155
		2	$y = -2772.8x - 7.9486$	0.9614	23.053	4.90×10	0.3051
		3	$y = -3629.6x - 6.0222$	0.9422	30.177	4.40×10^{1}	0.2331
	OS5	1	$y = -2530.8x - 8.8155$	0.9926	21.041	1.88×10	0.3343
		2	$y = -3282.4x - 7.1361$	0.9814	27.290	1.31×10^{1}	0.2577
		3	$y = -4151.4x - 5.2057$	0.9634	34.515	1.14×10^{2}	0.2038
648−923	OS1	1	$y = -1540.45x - 10.9239$	0.6181	12.807	1.39×10^{-1}	0.8413
		2	$y = -4786.1x - 5.7818$	0.5838	39.792	7.38×10^{1}	0.2708
		3	$y = -13087.6x + 6.4799$	0.6045	108.810	4.27×10^{7}	0.0990
	OS2	1	$y = -1092.44x - 11.3349$	0.3490	9.083	6.53×10^{-2}	1.1863
		2	$y = -4814.2x - 5.3829$	0.4082	40.025	1.11×10^{2}	0.2692
		3	$y = -12478.3x + 6.1802$	0.5461	103.745	3.01×10^{7}	0.1039
	OS3	1	$y = -2294.70x - 9.8986$	0.6792	19.078	5.76×10^{-1}	0.5648
		2	$y = -7676.9x - 1.8174$	0.6297	63.826	6.24×10^{3}	0.1688
		3	$y = -14694.9x + 8.6354$	0.6196	122.173	4.13×10^{8}	0.0882
	OS4	1	$y = -1319.79x - 10.7782$	0.6160	10.973	1.38×10^{-1}	0.9820
		2	$y = -5577.5x - 3.8143$	0.6036	46.371	6.15×10^{2}	0.2324
		3	$y = -6568.6x - 1.1336$	0.3239	54.611	1.06×10^{4}	0.1973
	OS5	1	$y = -792.10x - 11.6648$	0.2237	6.586	3.40×10^{-2}	1.6362
		2	$y = -4617.6x - 5.5156$	0.4309	38.391	9.29×10^{1}	0.2807
		3	$y = -9637.5x + 2.4582$	0.4669	80.126	5.63×10^{5}	0.1345

C−O content at 1090 cm^{-1} from aliphatic components of this sample was observed, and the benzene ring trisubstitution peak area of OS5, in the range of 700−900 cm^{-1}, accounted for nearly 75%. The results of TG−DTG showed that the WL of OS5 was higher than those of others and that the maximum WL rate was also higher, corresponding to its high V_d. Based on the kinetic analysis of CRm, it is concluded that the model for the pyrolysis kinetics of the OS1−OS5 sludge samples, for

https://doi.org/10.1021/acsomega.1c02734
ACS Omega 2021, 6, 27684−27696

the reaction order of n = 2, fits well, and the combustion reaction order is also selected at n = 2.

AUTHOR INFORMATION

Corresponding Author

Wenlong Mo − *State Key Laboratory of Chemistry and Utilization of Carbon Based Energy Resources and Key Laboratory of Coal Clean Conversion & Chemical Engineering Process (Xinjiang Uyghur Autonomous Region), College of Chemical Engineering, Xinjiang University, Urumqi, Xinjiang 830046, China;* orcid.org/0000-0003-3837-0915; Phone: 15022994903; Email: mowenlong@xju.edu.cn.Phone:

Authors

Xian-Kang Shan − *State Key Laboratory of Chemistry and Utilization of Carbon Based Energy Resources and Key Laboratory of Coal Clean Conversion & Chemical Engineering Process (Xinjiang Uyghur Autonomous Region), College of Chemical Engineering, Xinjiang University, Urumqi, Xinjiang 830046, China*

Xiaoqiang He − *State Key Laboratory of Chemistry and Utilization of Carbon Based Energy Resources and Key Laboratory of Coal Clean Conversion & Chemical Engineering Process (Xinjiang Uyghur Autonomous Region), College of Chemical Engineering, Xinjiang University, Urumqi, Xinjiang 830046, China;* orcid.org/0000-0001-9714-2571

Wen-Jie Qiang − *State Key Laboratory of Chemistry and Utilization of Carbon Based Energy Resources and Key Laboratory of Coal Clean Conversion & Chemical Engineering Process (Xinjiang Uyghur Autonomous Region), College of Chemical Engineering, Xinjiang University, Urumqi, Xinjiang 830046, China*

Xian-Yong Wei − *State Key Laboratory of Chemistry and Utilization of Carbon Based Energy Resources and Key Laboratory of Coal Clean Conversion & Chemical Engineering Process (Xinjiang Uyghur Autonomous Region), College of Chemical Engineering, Xinjiang University, Urumqi, Xinjiang 830046, China; Key Laboratory of Coal Processing and Efficient Utilization, China University of Mining & Technology, Ministry of Education, Xuzhou 221116 Jiangsu, China;* orcid.org/0000-0001-7106-4624

Bo Wei − *State Key Laboratory of Chemistry and Utilization of Carbon Based Energy Resources and Key Laboratory of Coal Clean Conversion & Chemical Engineering Process (Xinjiang Uyghur Autonomous Region), College of Chemical Engineering, Xinjiang University, Urumqi, Xinjiang 830046, China*

Xing Fan − *State Key Laboratory of Chemistry and Utilization of Carbon Based Energy Resources and Key Laboratory of Coal Clean Conversion & Chemical Engineering Process (Xinjiang Uyghur Autonomous Region), College of Chemical Engineering, Xinjiang University, Urumqi, Xinjiang 830046, China; College of Chemical and Biological Engineering, Shandong University of Science and Technology, Qingdao 266590 Shandong, China*

Yulong Wu − *State Key Laboratory of Chemistry and Utilization of Carbon Based Energy Resources and Key Laboratory of Coal Clean Conversion & Chemical Engineering Process (Xinjiang Uyghur Autonomous Region), College of Chemical Engineering, Xinjiang University, Urumqi, Xinjiang 830046, China; Institute of Nuclear and New Energy Technology, Tsinghua University, Beijing 100084, China;* orcid.org/0000-0003-0212-6689

Complete contact information is available at: https://pubs.acs.org/10.1021/acsomega.1c02734

Notes

The authors declare no competing financial interest.

ACKNOWLEDGMENTS

The authors sincerely acknowledge the financial support from the National Key Research and Development Program of China (2018YFC1902101), the Tianchi project for introducing high-level talents to Xinjiang Uyghur Autonomous Region (China), and the open project from Key Laboratory of Coal Processing and Efficient Utilization (China University of Mining and Technology), Ministry of Education.

REFERENCES

(1) Hu, G.; Feng, H.; He, P.; Li, J.; Hewage, K.; Sadiq, R. Comparative life-cycle assessment of traditional and emerging oily sludge treatment approaches. *J. Clean. Prod.* **2020**, *251*, 119594.

(2) Gong, Z.; Liu, C.; Wang, M.; Wang, Z.; Li, X. Experimental study on catalytic pyrolysis of oil sludge under mild temperature. *Sci. Total Environ.* **2020**, *708*, 135039.

(3) Hu, G.; Li, J.; Zeng, G. Recent development in the treatment of oily sludge from petroleum industry: a review. *J. Hazard. Mater.* **2013**, *261*, 470−490.

(4) Zhang, Z. Y.; Li, L. H.; Zhang, J. S.; Ma, C.; Wu, X. Solidification of oily sludge. *Petrol. Sci. Technol.* **2018**, *36*, 273−279.

(5) Ji, L.; Fu, X.; Wang, M.; Xu, C.; Chen, G.; Song, F.; Guo, S.; Zhang, Q. Enzyme cocktail containing NADH regeneration system for efficient bioremediation of oil sludge contamination. *Chemosphere* **2019**, *233*, 132−139.

(6) Yang, S. Q.; Zheng, X. M.; Wang, B. F. Analysis of pyrolysis kinetics of neighboring-portoil sludge. *CIESC J.* **2015**, *66*, 319−325.

(7) Zhao, M.; Wang, X.; Liu, D.; Li, Z.; Guo, S.; Zhu, W.; Shi, N.; Wen, F.; Dong, J. Insight into essential channel effect of pore structures and hydrogen bonds on the solvent extraction of oily sludge. *J. Hazard. Mater.* **2020**, *389*, 121826.

(8) Qin, L.; Han, J.; He, X.; Zhan, Y.; Yu, F. Recovery of energy and iron from oily sludge pyrolysis in a fluidized bed reactor. *J. Environ. Manage.* **2015**, *154*, 177−182.

(9) Xu, M.; Zhang, J.; Liu, H.; Zhao, H.; Li, W. The resource utilization of oily sludge by cogasification with coal. *Fuel* **2014**, *126*, 55−61.

(10) Zhou, L.; Jiang, X.; Liu, J. Characteristics of oily sludge combustion in circulating fluidized beds. *J. Hazard. Mater.* **2009**, *170*, 175−179.

(11) Gao, N.; Jia, X.; Gao, G.; Ma, Z.; Quan, C.; Naqvi, S. R. Modeling and simulation of coupled pyrolysis and gasification of oily sludge in a rotary kiln. *Fuel* **2020**, *279*, 118152.

(12) Huang, Q.; Wang, J.; Qiu, K.; Pan, Z.; Wang, S.; Chi, Y.; Yan, J. Catalytic pyrolysis of petroleum sludge for production of hydrogen-enriched syngas. *Int. J. Hydrogen Energy* **2015**, *40*, 16077−16085.

(13) Gong, Z.; Du, A.; Wang, Z.; Fang, P.; Li, X. Experimental study on pyrolysis characteristics of oil sludge with a tube furnace reactor. *Energy Fuels* **2017**, *31*, 8102−8108.

(14) Li, J.; Lin, F.; Xiang, L.; Zheng, F.; Che, L.; Tian, W.; Guo, X.; Yan, B.; Song, Y.; Chen, G. Hazardous elements flow during pyrolysis of oily sludge. *J. Hazard. Mater.* **2021**, *409*, 124986.

(15) Liu, W.-J.; Shao, Z.-G.; Xu, Y. Emission characteristics of nitrogen and sulfur containing pollutants during the pyrolysis of oily sludge with and without catalysis. *J. Hazard. Mater.* **2021**, *401*, 123820.

(16) Chen, G.; Li, J.; Li, K.; Lin, F.; Tian, W.; Che, L.; Yan, B.; Ma, W.; Song, Y. Nitrogen, sulfur, chlorine containing pollutants releasing

characteristics during pyrolysis and combustion of oily sludge. *Fuel* **2020**, *273*, 117772.
(17) Ma, Z.; Xie, J.; Gao, N.; Quan, C. Pyrolysis behaviors of oilfield sludge based on Py-GC/MS and DAEM kinetics analysis. *J. Energy Inst.* **2019**, *92*, 1053−1063.
(18) Liu, Y.; Yu, H.; Jiang, Z.; Song, Y.; Zhang, T.; Siyal, A. A.; Dai, J.; Bi, X.; Fu, J.; Ao, W.; Zhou, C.; Wang, L.; Li, X.; Jin, X.; Teng, D.; Fang, J. Microwave pyrolysis of oily sludge under different control modes. *J. Hazard. Mater.* **2021**, *416*, 125887.
(19) He, Q.; Huang, S. X.; Luo, W.; Su, Y. F.; Xia, M.; Zhou, N.; Zhou, Z. Study on the difference between in-situ and ex-situ catalytic pyrolysis of oily sludge. *Environ. Sci. Pollut. Res.* **2021**, DOI: 10.1007/s11356-021-14233-6.
(20) Mo, W.; Wu, Z.; He, X.; Qiang, W.; Wei, B.; Wei, X.; Wu, Y.; Fan, X.; Ma, F. Functional group characteristics and pyrolysis/combustion performance of fly ashes from Karamay oily sludge based on FT-IR and TG-DTG analyses. *Fuel* **2021**, *296*, 120669.
(21) Fernandez-Lopez, M.; Pedrosa-Castro, G. J.; Valverde, J. L.; Sanchez-Silva, L. Kinetic analysis of manure pyrolysis and combustion processes. *Waste Manage.* **2016**, *58*, 230−240.
(22) He, X.-Q.; Mo, W. L.; Wang, Q.; Ma, Y. Y.; Ma, F. Y.; Fan, X.; Wei, X. Y. Effect of swelling treatment by organic solvent on the structure and pyrolysis performance of the direct coal liquefaction residue. *Energy Fuels* **2020**, *34*, 8685.
(23) Song, A.; Zha, F.; Tang, X.; Chang, Y. Effect of the additives on combustion characteristics and desulfurization performance of cow dung briquette. *Chem. Eng. Process.* **2019**, *143*, 107585.
(24) Chen, J.; Mu, L.; Cai, J.; Yin, H.; Song, X.; Li, A. Thermal characteristics and kinetics of refining and chemicals wastewater, lignite and their blends during combustion. *Energy Convers. Manage.* **2015**, *100*, 201−211.
(25) Liu, Y.; Cao, X.; Duan, X.; Wang, Y.; Che, D. Thermal analysis on combustion characteristics of predried dyeing sludge. *Appl. Therm. Eng.* **2018**, *140*, 158−165.
(26) Zhang, Y.; Zhao, H.; Shi, Q.; Chung, K. H.; Zhao, S.; Xu, C. Molecular investigation of crude oil sludge from an electric dehydrator. *Energy Fuels* **2011**, *25*, 3116−3124.
(27) Pauchard, V.; Sjöblom, J.; Kokal, S.; Bouriat, P.; Dicharry, C.; Müller, H.; al-Hajji, A. Role of naphthenic acids in emulsion tightness for a low-total-acid-number (TAN)/highasphaltenes oil. *Energy Fuels* **2009**, *23*, 1269−1279.
(28) de Oliveira Silva, J.; Filho, G. R.; da Silva Meireles, C.; Ribeiro, S. D.; Vieira, J. G.; da Silva, C. V.; Cerqueira, D. A. Thermal analysis and FTIR studies of sewage sludge produced in treatment plantsThe case of sludge in the city of Uberlândia-MG. Brazil. *Thermochim. Acta* **2012**, *528*, 72−75.
(29) Zhu, X.; Yang, S.; Wang, L.; Liu, Y.; Qian, F.; Yao, W.; Zhang, S.; Chen, J. Tracking the conversion of nitrogen during pyrolysis of antibiotic mycelial fermentation residues using XPS and TG-FTIR-MS technology. *Environ. Pollut.* **2016**, *211*, 20−27.
(30) Wu, D.; Liu, G.; Sun, R. Investigation on structural and thermodynamic characteristics of perhydrous bituminous coal by fourier transform infrared spectroscopy and thermogravimetry/Mass spectrometry. *Energy Fuels* **2014**, *28*, 3024−3035.
(31) Ma, Y.-y.; Ma, F.-y.; Mo, W.-l.; Wang, Q. Five-stage sequential extraction of Hefeng coal and direct liquefaction performance of the extraction residue. *Fuel* **2020**, *266*, 117039−117048.
(32) Lin, X.; Wang, C.; Ideta, K.; Miyawaki, J.; Nishiyama, Y.; Wang, Y.; Yoon, S.; Mochida, I. Insights into the functional group transformation of a chinese brown coal during slow pyrolysis by combining various experiments. *Fuel* **2014**, *118*, 257−264.
(33) Wang, S.; Tang, Y.; Schobert, H. H.; Guo, Y. N.; Gao, W.; Lu, X. FTIR and simultaneous TG/MS/FTIR study of Late Permian coals from Southern China. *J. Anal. Appl. Pyrolysis* **2013**, *100*, 75−80.
(34) Qi, X.; Wang, D.; Xin, H.; Qi, G. In situ FTIR study of real-time changes of active groups guring Oxygen-Free reaction of coal. *Energy Fuels* **2013**, *27*, 3130−3136.
(35) Dun, W.; Liu, G. J.; Sun, R. Y.; Fan, X. Investigation of structural characteristics of thermally metamorphosed coal by FTIR spectroscopy and X-ray diffraction. *Energy Fuels* **2013**, *27*, 5823−5830.
(36) Ma, Y. Y.; Ma, F. Y.; Mo, W. L.; Fan, X. Influence of acid treatment on the structure and extraction performance of Xinjiang Hefeng low-rank coal. *J. Fuel Chem. Technol.* **2019**, *47*, 649−660.
(37) Schmidt, H.; Kaminsky, W. Pyrolysis of oil sludge in a fluidised bed reactor. *Chemosphere* **2001**, *45*, 285−290.
(38) Wang, Z.; Guo, Q.; Liu, X.; Cao, C. Low temperature pyrolysis characteristics of oil sludge under various heating conditions. *Energy Fuels* **2007**, *21*, 957−962.
(39) Jia, X. R.; Jin, B. S.; Li, R. TG-FTIR study on pyrolysis of sewage sludge. *Boiler Technol.* **2009**, *40*, 77−80.
(40) Scott, S.; Dennis, J.; Davidson, J.; Hayhurst, A. Thermogravimetric measurements of the kinetics of pyrolysis of dried sewage sludge. *Fuel* **2006**, *85*, 1248−1253.
(41) Wang, X.; Si, J.; Tan, H.; Niu, Y.; Xu, C.; Xu, T. Kinetics investigation on the combustion of waste capsicum stalks in Western China using thermogravimetric analysis. *J. Therm. Anal. Calorim.* **2012**, *109*, 403−412.
(42) Luo, R.; Zhou, Q. Combustion kinetic behavior of different ash contents coals co-firing with biomass and the interaction analysis. *J. Therm. Anal. Calorim.* **2017**, *128*, 567−580.
(43) Yan, M.; Zhou, X.; Zhang, S.; Liao, W.; Zhu, G.; Wang, J.; Kanchanatip, E.; Khan, M. S. Municipal solid waste pyrolysis under circulated pyrolytic gas atmosphere. *J. Mater. Cycles Waste Manag.* **2021**, *23*, 1141−1151.
(44) Wang, J.; Matsushita, T.; Yuminaga, J.; Jia, H. Study on the Preparation Method and Combustion Characteristics of Biomass Char Fuel Made from Chicken Manure Synergistic Plastic Waste. *IOP Conf. Ser.: Environ. Earth Sci.* **2021**, *696*, 012027.
(45) Zou, H.; Liu, C.; Evrendilek, F.; He, Y.; Liu, J. Evaluation of reaction mechanisms and emissions of oily sludge and coal co-combustions in O_2/CO_2 and O_2/N_2 atmospheres. *Renewable Energy* **2021**, *171*, 1327−1343.
(46) Li, S. F.; Fang, M. X.; Li, X. W. Ignition and combustion characteristics of multi-generation semi-coke under pressurization. *J. Combust. Sci. Technol.* **2012**, *18*, 27−32.

https://doi.org/10.1021/acsomega.1c02734
ACS Omega 2021, 6, 27684−27696